Original Article

The effect of post-labeling delay on cerebral blood flow is influenced by age and sex: a study based on arterial spin-labeling magnetic resonance imaging

Ying Hu[1,2], Kai Zhang[1], Rongbo Liu[1]

[1]Department of Radiology, West China Hospital, Sichuan University, Chengdu, China; [2]West China Biomedical Big Data Center, West China Hospital, Sichuan University, Chengdu, China

Contributions: (I) Conception and design: Y Hu, R Liu; (II) Administrative support: Y Hu, R Liu; (III) Provision of study materials or patients: Y Hu, K Zhang; (IV) Collection and assembly of data: Y Hu, K Zhang; (V) Data analysis and interpretation: All authors; (VI) Manuscript writing: All authors; (VII) Final approval of manuscript: All authors.

Correspondence to: Ying Hu, MD. Department of Radiology, West China Hospital, Sichuan University, Chengdu, China; West China Biomedical Big Data Center, West China Hospital, Sichuan University, No. 37 Guoxue Alley, Chengdu 610041, China. Email: yinghu@wchscu.cn.

Background: Whether the effect of post-labeling delay (PLD) on cerebral blood flow (CBF) is influenced by age and sex in adults is unknown. In this study, we mainly aimed to explore the potential influence of age and sex on the effect of PLD on CBF.

Methods: This prospective study enrolled 90 healthy adult volunteers (49.47±15.63 years of age; age range, 20–77 years; 47 female; 43 male). All participants underwent 3-dimensional (3D) pseudo-continuous arterial spin labeling (ASL) imaging with 3 different PLDs (1,525, 2,025, and 2,525 ms). The CBF values for each PLD, the arterial transit time (ATT), and the spatial coefficient of variation (spatial CoV) were computed for 21 regions of interest (ROIs) in every participant. Multivariate regression analysis was conducted to assess the potential influence of age and sex on the effect of PLD on CBF and the relationships among CBF, ATT, PLD, age, sex, and spatial CoV.

Results: The CBF increased for 7.32 to 9.87 mL/100 g/min as the PLD increased per 1 second in the global gray matter, bilateral frontal, temporal lobes, the vascular territories of bilateral anterior and middle carotid artery. When the age increased per 1 year, the speed of the changes for CBF decreased for 0.26 to 0.3 mL/100 g/min/s in these regions. However, the CBF decreased for 12 to 17 mL/100 g/min as the PLD increased per 1 second in the bilateral limbic lobes, insula, and deep gray matter. In these regions, the speed of the changes for CBF increased for 0.2 to 0.28 mL/100 g/min/s as the age increased per 1 year. Furthermore, compared to the female, the speed of the changes for CBF decreased for 3.58 to 4.6 mL/100 g/min/s for the male in global gray matter, bilateral frontal, limbic lobes, and the vascular territories of bilateral anterior carotid artery, and the speed increased 4.49 to 5.09 mL/100 g/min/s for the male in the limbic lobes. In addition, the CBF decreased with aging and the CBF tended to be higher in females compared to males. At the same time, we found that the ATT of all ROIs increased with age and manifested higher in males than females. Moreover, we found that CBF decreased with the increase of ATT, and the effect of ATT on CBF was less influenced by PLD. Finally, we found that the spatial CoV of ASL in certain regions increased with the increase of ATT and age, and was greater in males.

Conclusions: The effect of PLD on CBF can be influenced by age and sex. The relationships among CBF, ATT, PLD, age, sex, and spatial CoV found in this study may have certain significance for the study of ASL imaging in the future.

Keywords: Arterial spin-labeling; cerebral blood flow (CBF); post-labeling delay (PLD); arterial transit time (ATT); interaction effect

Introduction

Cerebral blood flow (CBF) refers to the rate at which arterial blood is delivered to the capillary bed in brain tissue (1). It serves as an important physiological indicator of cerebral metabolism and functional activity (2) and can be utilized as a biomarker for neurodegenerative diseases (3) and neurological dysfunction (4-6). Arterial spin labeling (ASL) is a noninvasive magnetic resonance (MR) perfusion imaging technique that employs water in the blood as an endogenous tracer for quantifying CBF (7-9). The ASL MR imaging (MRI) has a wide range of clinical availability and demand (10-12). The post-labeling delay (PLD) and the inversion time are critical parameters in ASL, representing the time between labeling and acquisition, and directly impacting the accuracy of CBF quantification (7,13-16).

The use of a single PLD is common (9) as it allows for a short scanning time and robust and reliable CBF measurements. Therefore, a single-PLD approach is recommended as the clinical standard scanning protocol in the guideline published in 2015 (9). Although 2 seconds is the suggested PLD for the clinical adult population in this guideline, previous studies have employed various PLD protocols (9,17-19), and the commonly used PLDs in recent studies have ranged from 1.5 to 2.5 seconds (11,18-23). In addition, a guidance published in 2023 states that many studies and clinical experiences have shown that the 2015 consensus PLD of 1,800–2,000 ms may not be sufficient for all the labeled blood to arrive in the brain parenchyma (10). Given the importance of PLD for quantifying CBF using ASL and the lack of uniformity in PLDs in current research, several studies have aimed to optimize the PLD for ASL imaging (7,9,24). Nonetheless, there has been a paucity of research on optimizing PLD based on age. van der Thiel *et al.* noted the challenge of modifying the optimal PLD across the lifespan (7). A possible reason for this challenge is the difficulty in recruiting participants spanning all age groups. Therefore, it is crucial to investigate whether there is an age range in which CBF values are more sensitive to changes in PLD. Identifying these specific age groups would enable researchers to focus their attention on these critical periods. Another challenge in choosing the optimal PLD may be that arterial transit time (ATT) changes depending on the region of the brain (25,26), whereas in ASL imaging, the most ideal PLD is matched with ATT. Therefore, the ideal PLD is a compromise, as we are trying to image the brain at a time when enough labeled spins have traveled to the tissue, and signal-to-noise ratio is still high enough. Although there have been many studies to measure ATT (26-31), few studies have explored the effects of age and sex on ATT using larger normal population samples. In addition, due to the mismatch between ATT and PLD, ATT artifacts usually appear in ASL imaging. The spatial coefficient of variation (spatial CoV) in ASL may be used to evaluate and quantify ATT artifacts, because the ASL signal is spatially homogeneous when there is no ATT artifact, whereas the ASL signal is different between vascular and tissue regions when ASL tracer has not arrived in the tissue yet (32).

Previous studies have demonstrated the impact of PLD on CBF measurements (7,13). However, to date, there is a dearth of research investigating whether the influence of PLD on CBF is influenced by age and sex. Therefore, we aimed to include a comprehensive sample of adults with a relatively wide age range to examine the effect of PLD on CBF in the whole brain and specific brain regions, and to explore the potential interactions between PLD and age, as well as between PLD and sex. In addition, we calculated the ATT of each brain region and explored the effects of age and sex on ATT and the effect of ATT on CBF. Furthermore, we investigated the effect of ATT, PLD, and age on the spatial CoV. We hope this study will provide valuable insights for optimizing ASL imaging technique. We present this article in accordance with the STROBE reporting checklist (available at https://qims.amegroups.com/article/view/10.21037/qims-23-1622/rc).

Methods

Participants

This prospective study was conducted in accordance with the Declaration of Helsinki (as revised in 2013) and approved by the Institutional Review Board of West China Hospital of Sichuan University (No. 2021[818]), and all participants provided written informed consent. We conducted the Mini-Mental State Examination (MMSE)

Table 1 Demographic data of our examined study sample

Group	Age range (years)	N (%)	Gender (F/M)	Age (mean ± SD) (years)
Youth group	20–45	31 (34.44)	16/15	31.10±8.19
	20–25	11 (12.22)	6/5	
	26–30	7 (7.78)	3/4	
	31–35	3 (3.33)	2/1	
	36–40	3 (3.33)	1/2	
	41–45	7 (7.78)	4/3	
Middle-aged group	46–60	33 (36.67)	17/16	53.09±4.29
	46–50	12 (13.33)	5/7	
	51–55	10 (11.11)	6/4	
	56–60	11 (12.22)	6/5	
Elderly group	61–77	26 (28.89)	14/12	66.77±4.73
	61–65	14 (15.56)	7/7	
	66–70	6 (6.67)	3/3	
	71–77	6 (6.67)	4/2	
Total	20–77	90 (100)	47/43	49.47±15.63

Data are the numbers of volunteers. F, female; M, male; SD, standard deviation.

and Mattis Dementia Rating Scale (MDRS) and selected individuals with scores above 24 on the MMSE and above 130 on the MDRS. A total of 103 individuals with normal cognition, who had no history of brain tumor, trauma, brain injury, cerebrovascular disorder, carotid stents or dentures, neurologic or cardiac disease, hypertension, diabetes, renal disease, alcoholism, or metal implants in the body, were selected for this study. One participant was excluded because of claustrophobia.

After the magnetic resonance imaging (MRI) examination, 2 experienced neuro-radiologists inspected the conventional MRI, MR angiography (MRA), and the raw pseudo-continuous arterial spin labeling (pCASL) images to identify any intracranial lesions (3 participants) or vascular lesions (9 participants) or obvious motion or ATT artifacts. Subsequently, a total of 90 right-handed healthy adults (49.47±15.63 years of age; age range, 20–77 years; female: 47; male: 43) were enrolled in the study. Additionally, these participants were divided into 3 age groups: the youth group, the middle-aged group, and the elderly group. The age distributions of the participants are listed in *Table 1*. All participants refrained from alcohol, caffeine, nicotine, and vigorous exercise for 24 hours prior to the MRI.

MRI acquisition

Imaging was conducted using a 3.0-T MR scanner (Signa HDxt; GE Healthcare, Chicago, IL, USA) equipped with an 8-channel head coil. Conventional MR sequences, including axial T2-weighted, axial fluid-attenuated inversion recovery, and axial 3-dimensional (3D) T1-weighted sequences were acquired to identify participants with intracranial lesions. Phase-contrast MRA was performed to exclude cases with any cerebrovascular lesions. Perfusion images were obtained using pCASL imaging with 3 PLDs. The imaging protocol involved a 3D background-suppressed fast-spin-echo acquisition with the following parameters: 3 PLDs of 1,525 ms, 2,025 ms, and 2,525 ms; repetition time of 4,521 ms (PLD 1,525 ms), 4,912 ms (PLD 2,025 ms), and 5,216 ms (PLD 2,525 ms); echo time of 9.8 ms; number of excitations of 3; field of view (FOV) of 24×24 cm^2; reconstructed matrix of 64×64; section thickness of 4 mm; number of sections of 30; sampling points on 8 spirals, 512; labeling duration of 1,525 ms; and acquisition times of 4 minutes and 22 seconds (PLD 1,525 ms), 4 minutes and 52 seconds (PLD 2,025 ms), and 5 minutes and 8 seconds (PLD 2,525 ms). A proton density-weighted image (M0) was acquired on participants using the same acquisition

parameters as the pCASL and the pre-saturation pulse but without the labeling.

MRI analysis

All imaging data analyses were conducted using MATLAB R2014a (MathWorks, Natick, MA, USA), statistical parametric mapping (SPM8) software (http://www.fil.ion.ucl.ac.uk/spm/software/spm8/), ADW4.5 (GE workstation), and WFU Pickatlas (http://fmri.wfubmc.edu/software/PickAtlas).

The raw pCASL images were checked for gross head motion: translations greater than 3 mm and rotations greater than 3° as defined by Wang *et al.* (33). Then, the raw ASL data was realigned to the M0 volume which presents equilibrium magnetization using SPM8. The raw images were then smoothed with an isotropic Gaussian kernel (6 mm full width at half maximum). The T1-weighted images were skull stripped using FSL (FMRIB Software Library, Oxford, United Kingdom) and segmented using the unified segmentation method (34).

We calculated the ATT using a weighted-delay (WD) method (27) as follows:

$$WD(\delta) = \frac{\sum_{i=1}^{n} w_i \cdot \Delta M(\delta, w_i)}{\sum_{i=1}^{n} \Delta M(\delta, w_i)} \qquad [1]$$

where w_i (i=1,…,n) is the PLD of each scan and ΔM (δ, w_i) is the ASL signal of each bolus with a transit time delay δ at the PLD w_i. Previous studies have shown that the WD was found to be a simple monotonic function of assumed delay. The transit delay, ATT, could be calculated numerically inverted from WD (27).

CBF maps were generated from raw ASL images using ADW4.5 (GE workstation). The quantitative CBF map was acquired after the pair-wise subtraction of labeled and non-labeled images. The CBF quantification (in mL/100 g/min) was calculated with the equation (32,35):

$$CBF = \frac{\lambda \left(1 - \exp(-2.0s / 1.2s)\right) \cdot \exp\left(PLD / T_{1blood}\right)}{2\alpha T_{1blood}\left(1 - \exp\left(-TL / T_{1blood}\right)\right)} \cdot \frac{\Delta S}{S_0} \qquad [2]$$

where λ is the tissue blood partition coefficient of water (0.9 mL/g), PLD is the post-label delay, T_{1blood} is the arterial blood water relaxation time at 3T (1.664 s), α is the labeling efficiency (0.85), TL is the labeling duration, ΔS is the ASL difference signal, and S_0 is the proton-density signal intensity. The term (1–exp(–2.0 s/1.2 s)) in the numerator reflects the

presence of a saturation pulse that is applied in the proton-density images and allows conversion between measured MR signal (S0) and the unperturbed longitudinal gray matter magnetization (36,37). The 2 s in this term indicates the saturation, the 1.2 s in this term is the T1 of grey matter.

The CBF maps were registered to their respective skull-stripped T1-weighted images using a rigid body transformation and spatially normalized to the Montreal Neurological Institute template. Finally, the CBF maps were smoothed with an isotropic Gaussian kernel (6 mm full width at half maximum). The masks of global gray matter, bilateral frontal, parietal, temporal, occipital, limbic lobes, insula, and deep gray matter were generated using WFU Pickatlas. In addition, we generated the masks for the vascular territories of the bilateral anterior, middle, and posterior carotid artery (38-41). Finally, the CBF of the above 21 regions of interest (ROIs) were extracted from the preprocessed CBF maps using the corresponding masks.

The spatial CoV for the global gray matter, bilateral frontal lobes, bilateral parietal lobes, bilateral temporal lobes, bilateral occipital lobes, bilateral limbic lobes, bilateral deep gray matter, and the vascular territories of the anterior, middle, and posterior carotid artery were obtained using the method described in previous study (32). The spatial CoV was defined as the standard deviation of CBF divided by the mean CBF, within an ROI:

$$Spatial\ CoV_{ROI} = \frac{\sigma\left(CBF_{ROI}\right)}{\mu\left(CBF_{ROI}\right)} \times 100\% \qquad [3]$$

Statistical analysis

The statistical analysis was conducted using Stata (version 15.0; StataCorp, College Station, TX, USA). We performed multivariate linear regression to investigate the potential influence of age and sex on the effect of PLD on CBF. The dependent variable was CBF; the independent variables included PLD, the interaction term between PLD and age (PLD multiplied by age), and the interaction term between PLD and sex (PLD multiplied by sex). Sex and age were included as control variables. In addition, we evaluated the ATT changes due to age and sex, the effect of ATT on CBF, and the association of ATT, PLD and age with the spatial CoV.

The statistical analysis equations were expressed as follows:

$$CBF = \beta_1 PLD + \beta_2 age + \beta_3 sex + \beta_4 PLD * age \qquad [4]$$
$$+ \beta_5 PLD * sex + constant$$
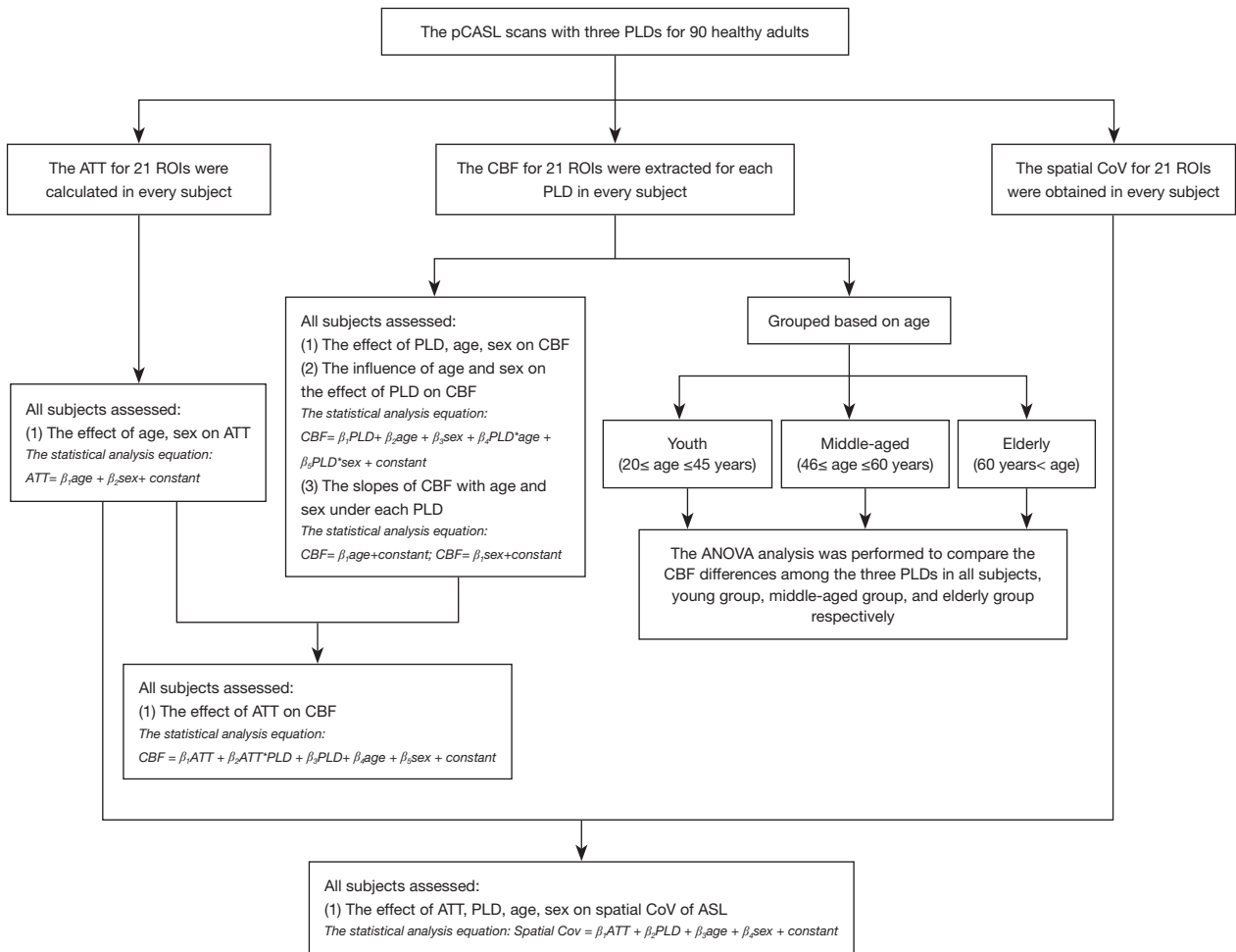
Figure 1 Study process. pCASL, pseudo-continuous arterial spin labeling imaging; PLD, post-labeling delay; ATT, arterial transit time; ROI, region of interest; CBF, cerebral blood flow; spatial CoV, spatial coefficient of variation; ANOVA, analysis of variance.

$$ATT = \beta_1 age + \beta_2 sex + constant \qquad [5]$$

$$CBF = \beta_1 ATT + \beta_2 ATT * PLD + \beta_3 PLD + \beta_4 age + \beta_5 sex + constant \qquad [6]$$

$$Spatial\ CoV = \beta_1 ATT + \beta_2 PLD + \beta_3 age + \beta_4 sex + constant \qquad [7]$$

In the regression analysis, β(n) represents the regression coefficients. Sex was coded as 0 for female and 1 for male. A P value less than 0.05 was considered statistically significant.

In addition, to compare the changes of CBF with age and sex under different PLD, we used regression analysis to calculate the slopes of CBF with age and sex under each PLD. Furthermore, we compared the mean CBF across the 3 PLDs to determine the approximate trend of CBF for each region. Differences among the CBF values of the 3 PLDs were assessed using one-way analysis of variance (ANOVA) with Scheffe post hoc analysis. The ANOVA was conducted for all participants regardless of age group, as well as for the young group (20–45 years), middle-aged group (46–60 years), and elderly group (>60 years), respectively.

We used the Bonferroni adjustment method to correct the multiple comparisons (42). The Bonferroni adjustment requires the alpha level for each individual comparison be equal to 5% divided by the total number of the comparisons (43). Therefore, to get a more conservative result, in this study, a P value less than 0.01 was considered statistically significant in the multivariate linear regression and ANOVA, and a P value less than 0.005 was considered to indicate a statistically significant difference in the Scheffe post hoc analysis. The detailed analysis process is illustrated in *Figure 1*.

Table 2 The results of regression analysis about the effect of PLD on CBF

ROIs	PLD	Age	Sex	PLD*age	PLD*sex
Global GM	0.00732 (0.005)	−0.69182 (<0.001)	−10.24805 (0.001)	−0.00026 (<0.001)	−0.00389 (0.002)
Frontal lobe_L	0.00893 (0.003)	−0.83804 (<0.001)	−9.49887 (0.008)	−0.0003 (<0.001)	−0.00358 (0.002)
Frontal lobe_R	0.00971 (0.001)	−0.8439 (<0.001)	−11.32288 (0.003)	−0.0003 (<0.001)	−0.0046 (0.002)
Parietal lobe_L	0.00514 (0.074)	−0.67939 (<0.001)	−10.97641 (0.006)	−0.00023 (<0.001)	−0.00467 (0.013)
Parietal lobe_R	0.00614 (0.046)	−0.66904 (<0.001)	−12.38452 (0.002)	−0.00025 (<0.001)	−0.00533 (0.004)
Temporal lobe_L	0.00987 (0.002)	−0.80725 (<0.001)	−8.28237 (0.008)	−0.00029 (<0.001)	−0.00278 (0.109)
Temporal lobe_R	0.00877 (0.006)	−0.78684 <0.001)	−10.07556 (0.005)	−0.00028 (<0.001)	−0.00392 (0.019)
Occipital lobe_L	0.00406 (0.208)	−0.54782 (<0.001)	−15.67818 (<0.001)	−0.00022 (<0.001)	−0.00547 (0.004)
Occipital lobe_R	0.00244 (0.453)	−0.52795 (<0.001)	−14.82482 (<0.001)	−0.0002 (0.001)	−0.00531 (0.002)
Limbic lobe_L	−0.01344 <0.001)	−0.65760 (<0.001)	−12.16350 (0.003)	−0.00023 (<0.001)	−0.00449 (0.001)
Limbic lobe_R	−0.01208 (<0.001)	−0.56707 (<0.001)	−13.14530 (0.001)	−0.0002 (<0.001)	−0.00509 (0.004)
Insula_L	−0.0173 (<0.001)	−0.84812 (<0.001)	−3.39832 (0.465)	−0.00026 (<0.001)	−0.00117 (0.58)
Insula_R	−0.01862 (<0.001)	−0.94827 (<0.001)	−4.29838 (0.364)	−0.00028 (<0.001)	−0.00177 (0.409)
Deep GM_L	−0.01679 (<0.001)	−0.60387 (<0.001)	−5.59111 (0.07908)	−0.00025 (<0.001)	−0.00228 (0.13837)
Deep GM_R	−0.01727 (<0.001)	−0.64652 (<0.001)	−5.90463 (0.06820)	−0.00026 (<0.001)	0.00249 (0.11159)
ACA_L	0.00948 (0.001)	−0.77552 (<0.001)	−10.1879 (0.004)	−0.00027 (<0.001)	−0.00389 (0.003)
ACA_R	0.00973 (0.001)	−0.81679 (<0.001)	−11.332 (0.002)	−0.00028 (<0.001)	−0.0046 (0.009)
MCA_L	0.00884 (0.003)	−0.77442 (<0.001)	−8.9891 (0.004)	−0.00028 (<0.001)	0.00326 (0.059)
MCA_R	0.00875 (0.002)	−0.7511 (<0.001)	−11.301 (0.001)	−0.00027 (<0.001)	−0.0044 (0.018)
PCA_L	0.0076 (0.016)	−0.580 (<0.001)	−14.606 (<0.001)	−0.00023 (<0.001)	−0.00513(0.006)
PCA_R	0.00584 (0.042)	−0.5336 (<0.001)	−14.106 (<0.001)	−0.0002 (<0.001)	−0.0051 (0.003)

The regression coefficients listed in the form are non-standardized regression coefficients (the statistical analysis equation was as follows: CBF = β_1PLD + $\beta_2$age + $\beta_3$sex + β_4PLD*age + β_5PLD*sex + constant). The P values of the regression coefficients are listed in parentheses in this table. P<0.01 is statistically significant. "L" stands for the left lateral of the brain; "R" stands for the right lateral of the brain. PLD, post-labeling delay; CBF, cerebral blood flow; ROIs, regions of interest; GM, gray matter; ACA, anterior carotid artery; MCA, middle carotid artery; PCA, posterior carotid artery.

In this study, we used PASS (version 21.0.3; NCSS, LLC, East Kaysville, UT, USA) software to estimate the sample size. For sample size estimation of multiple regression, we set the following parameters in PASS software: power calculation method: Conditional (Recommended)-Uses R^2; Power =0.9; Alpha =0.01; K=1; R^2(T/C) =0.2425; L=4; R^2(C) =0.1844. The sample size required for multiple regression analysis was estimated to be 40. For sample size estimation of ANOVA, we set the following parameters in PASS software: Power =0.9; Alpha =0.005; G (Number of Groups) =3; Group Allocation Input Type: Equal; µ1: 37.23, 39.76, 44.29; σ=5.86. The sample size required for multiple regression analysis was estimated to be 84.

Results

The effect of PLD on CBF

The CBF for all ROIs is expressed as the mean ± standard deviation in Table S1. The result of the regression analysis indicated that the CBF increased with the increase of PLD in the global gray matter, bilateral frontal, temporal lobes, and the vascular territories of bilateral anterior and middle carotid artery (β ranged from 0.00732 to 0.00987). In this regression analysis, β was a non-standardized regression coefficient. Therefore, in these ROIs, among the ranges of PLDs we adopted, the CBF increased for 7.32 to 9.87 mL/100 g/min as the PLD increased per

Table 3 The summary of ANOVA

Rough trends of CBF changing	Group	ROIs with statistical significant in ANOVA
CBF1 < CBF2 < CBF3	ALL	Global GM, Frontal lobe_L, Frontal lobe_R, Parietal lobe_L Parietal lobe_R, Temporal lobe_L, Temporal lobe_R, Occipital lobe_L, Occipital lobe_R, ACA_L, ACA_R, MCA_L, MCA_R, PCA_L, PCA_R
	Y	–
	M	Global GM, Frontal lobe_L, Frontal lobe_R, Parietal lobe_L, Parietal lobe_R, Temporal lobe_L, Temporal lobe_R, Occipital lobe_L, Occipital lobe_R, ACA_L, ACA_R, MCA_L, MCA_R, PCA_L, PCA_R
	O	Global GM, Frontal lobe_L, Frontal lobe_R, Parietal lobe_L, Parietal lobe_R, Temporal lobe_L, Temporal lobe_R, Occipital lobe_L, Occipital lobe_R, ACA_L, ACA_R, MCA_L, MCA_R, PCA_L, PCA_R
CBF3 < CBF2 < CBF1	ALL	–
	Y	Limbic lobe_L, Limbic lobe_R, Insula_L, Insula_R, Deep GM_L, Deep GM_R
	M	–
	O	–
CBF2 < CBF3 < CBF1	ALL	Insula_L, Insula_R, Deep GM_L, Deep GM_R
	Y	–
	M	Deep GM_L, Deep GM_R
	O	–

"ALL" indicates all participants (age range, 20–77 years). "Y" indicates youth group (age range, 20–45 years). "M" indicates middle-aged group (age range, 46–60 years). "O" indicates elderly group (age range, 61–77 years). unit: mL/100 g/min. GM, gray matter. "L" stands for the left lateral of the brain; "R" stands for the right lateral of the brain. CBF1 is the CBF when the PLD is 1,525 ms; CBF2 is the CBF when the PLD is 2,025 ms; CBF3 is the CBF when the PLD is 2,525 ms. ANOVA, analysis of variance; CBF, cerebral blood flow; ROIs, regions of interest; ACA, anterior carotid artery; MCA, middle carotid artery; PCA, posterior carotid artery; GM, gray matter; PLD, post-labeling delay.

1 second. However, the CBF decreased with the increase of PLD in bilateral limbic lobes, insula, and deep gray matter (β ranged from –0.017 to –0.012). Thus, in these ROIs, among the ranges of PLDs we adopted, CBF decreased for 12 to 17 mL/100 g/min as the PLD increased per 1 second. The detailed regression coefficients for PLD in all ROIs are listed in *Table 2*.

When the participants were not grouped, ANOVA revealed significant differences of CBF among different PLDs in all ROIs except bilateral limbic lobes. For the youth group, the ANOVA analysis showed significant differences of CBF among different PLDs in bilateral limbic lobes. The mean values of CBF in global gray matter, bilateral frontal, parietal, temporal, occipital lobes, the vascular territories of bilateral anterior, middle, and posterior carotid artery roughly demonstrated a pattern as follows: $CBF_{PLD=1,525 ms} < CBF_{PLD=2,025 ms} < CBF_{PLD=2,525 ms}$. The other pattern showed lower CBF with PLD of 2,025 ms compared to the CBF with PLD of 1,525 and 2,525 ms. The brain regions that showed this pattern included the bilateral insula, deep gray matter, and limbic lobes. *Table 3* displays the ROIs with statistically significant results in the ANOVA. Table S1 provides detailed ANOVA analysis results and approximate trend of CBF. *Figure 2* displays boxplots of CBF for some brain regions.

The effect of PLD on CBF was influenced by age

The interaction term (PLD*Age) was negatively correlated with CBF in all ROIs. The regression coefficients of this interaction term ranged from –0.0003 to –0.00026 in global gray matter, bilateral frontal, temporal lobes, and the vascular territories of bilateral anterior and middle carotid artery. Within these brain regions, PLD was positively correlated with CBF. Therefore, in these brain regions, individuals with elder age exhibited a smaller increase in CBF with PLD increasing. Specifically, when the age increased per 1 year, the speed of the changes for CBF decreased by 0.26 to 0.3 mL/100 g/min/s.

The regression coefficients of the above interaction
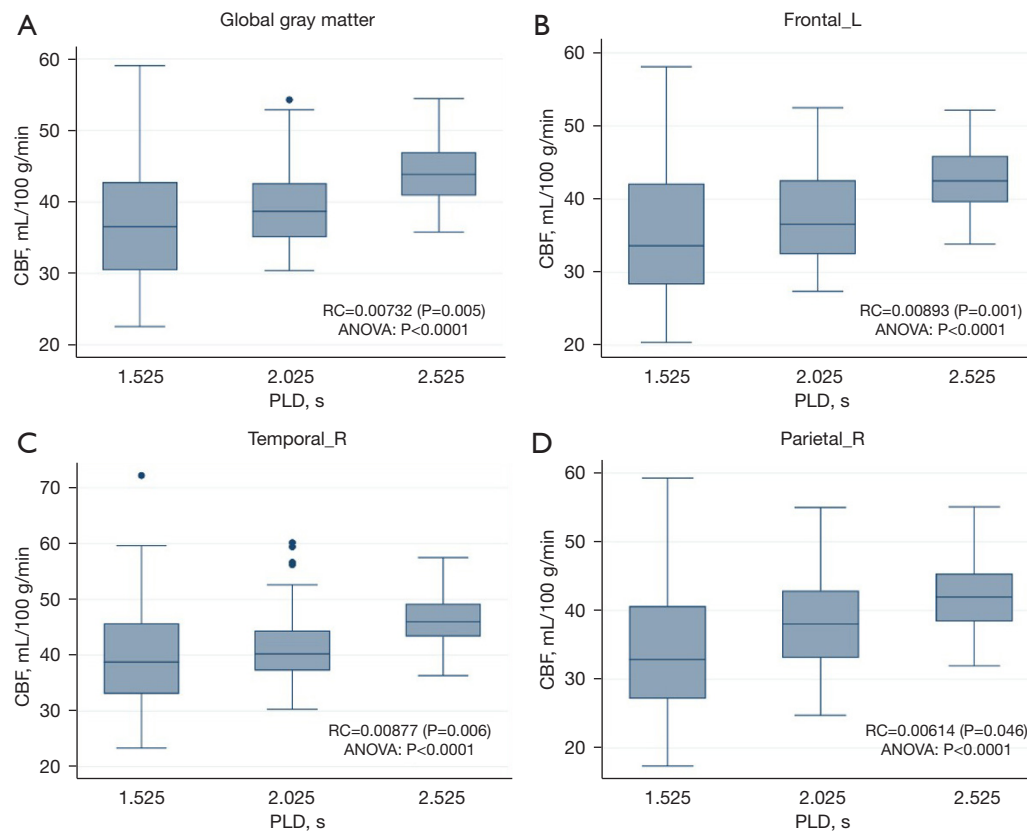
Figure 2 The boxplot of CBF values in some brain regions under three PLDs. The figure shows the CBF of global gray matter (A), left frontal lobe (B), right temporal lobe (C), right parietal lobe (D) showed a gradually increasing trend in the 3 PLDs (1.525, 2.025, 2.525 s); the RCs in these regions were positive and statistically significant; and the ANOVA of cerebral blood flow under the 3 PLDs in these regions were statistically significant. The black dots in this figure were discrete values. CBF, cerebral blood flow; RC, regression coefficient; ANOVA, analysis of variance; PLD, post-labeling delay.

term ranged from –0.00028 to –0.0002 in bilateral limbic lobes, insula, and deep gray matter. Conversely, PLD was negatively correlated with CBF in these regions. Thus, in these brain regions, individuals with elder age exhibited a larger decrease in CBF with PLD increasing. Specifically, when the age increased per 1 year, the speed of the changes for CBF increased by 0.2 to 0.28 mL/100 g/min/s. The detailed regression coefficients for PLD*age in all ROIs are listed in *Table 2*. *Figure 3* displays the scatter plots for the changes of CBF with the interaction term (PLD*age) in some brain regions.

The effect of PLD on CBF was influenced by sex

The interaction term (PLD*sex) was negatively correlated with CBF in the global gray matter ($\beta=-0.00389$), bilateral

frontal ($\beta=-0.0035$ and -0.0046), limbic lobes ($\beta=-0.00449$ and -0.00509), and the vascular territories of bilateral anterior carotid artery ($\beta =-0.00389$ and -0.0046). The PLD was positively correlated with CBF in global gray matter, bilateral frontal, and the vascular territories of bilateral anterior carotid artery. In this study, males were coded as 1 and females as 0. Therefore, compared to the female, the speed of the changes for CBF decreased by 3.58 to 4.6 mL/100 g/min/s for the male in the above brain regions. However, The PLD was negatively correlated with CBF. Thus, compared to the female, the speed of the changes for CBF increased by 4.49 to 5.09 mL/100 g/min/s for the males in the limbic lobes. The detailed regression coefficients for PLD*sex in all ROIs are listed in *Table 2*. *Figure 4* presents the box plots of CBF at different values of the interaction term (PLD*sex) in some brain regions.

4396

Hu et al. Age and sex influence the effect of PLD on CBF
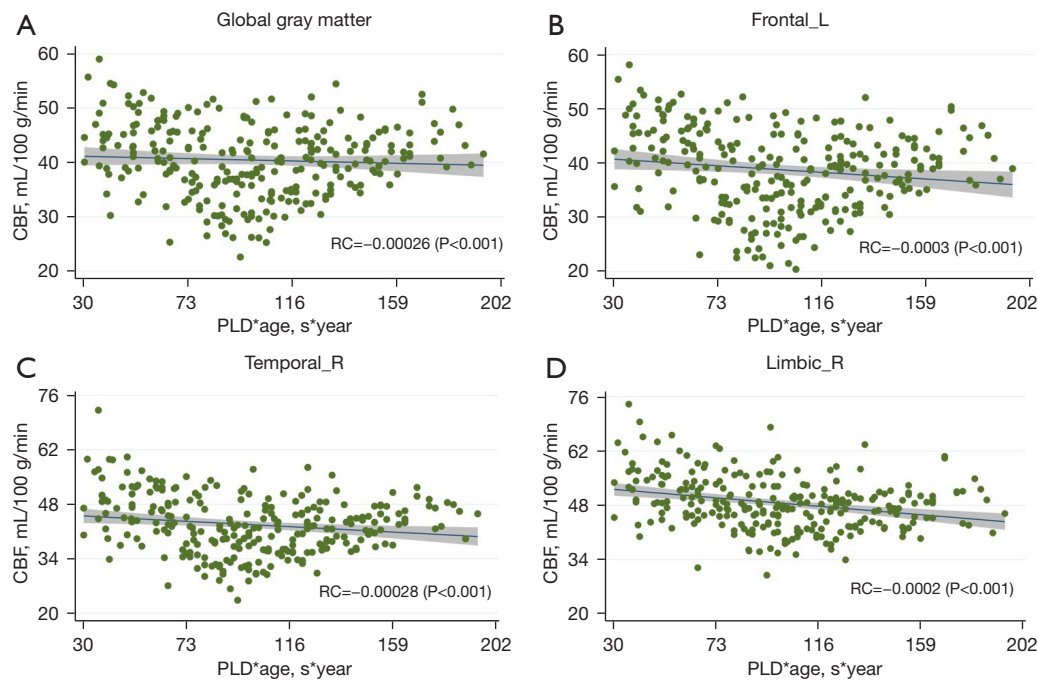
Figure 3 The Scatterplot of CBF values in some brain regions under different values of the interaction term (PLD*age). In this study, the relationship between CBF and PLD can be expressed by the following equation: CBF = β_1PLD + β_2PLD*age + β_3PLD*sex. Therefore, for the same sex, the variation of CBF with PLD is determined by the regression coefficient β_1 plus β_2 and age. The figure shows that the regression coefficient β_1 in the global gray matter (A), left frontal lobe (B), right temporal lobe (C), right limbic lobe (D) is positive, and the regression coefficient β_2 were negative, so in these brain regions, the changes of CBF with PLD in younger were greater than that of older. CBF, cerebral blood flow; PLD, post-labeling delay; RC, regression coefficient.

The effect of age and sex on CBF

The regression analysis results indicated that the CBF decreased with aging in all ROIs (β ranged from –0.948 to –0.528). Therefore, we simply speculated that with the age increase per year, CBF decreased by 0.528 to 0.948 mL/100 g/min. In addition, the CBF tended to be higher in females compared to males in all ROIs (β ranged from –15.678 to –8.282) except for the bilateral insula and deep gray matter.

In addition, we calculated the slopes of CBF with age and sex under different PLDs. We found that the slopes of CBF with age were statistically significant in almost all ROIs when the PLD was 1,525 and 2,025 ms, and the slopes of CBF with age were largest with the PLD of 1,525 ms among the 3 PLDs (1,525, 2,025, 2,525 ms). However, the slopes of CBF with sex were statistically significant when the PLD was 1,525 ms and were not statistically significant when the PLD were 2,025 ms or 2,525 ms in most ROIs. This may indicate that the measurement results of the slopes for CBF with age were more susceptible to PLD

changes compared to the slopes for CBF with sex.

As for the slope of CBF with age, the differences of the slopes among the 3 PLDs were larger in frontal, temporal, and the territories of anterior and middle cerebral arteries (the differences of the absolute value for the slopes ranged from 0.267 to 0.3) than that in the parietal, occipital, and the territories of posterior cerebral arteries (the differences of the absolute value for the slopes ranged from 0.197 to 0.262). The slopes of CBF with age and sex under different PLDs are listed in Table S2.

The effect of age and sex on ATT

The results of the regression analysis showed that the ATT of all ROIs were positively significant related to the age (β ranged from 0.364 to 0.597). The ATT were higher in males than the females in all ROIs except for bilateral insula (β ranged from 0.137 to 0.371). Detailed results of regression analysis can be found in Table S3.
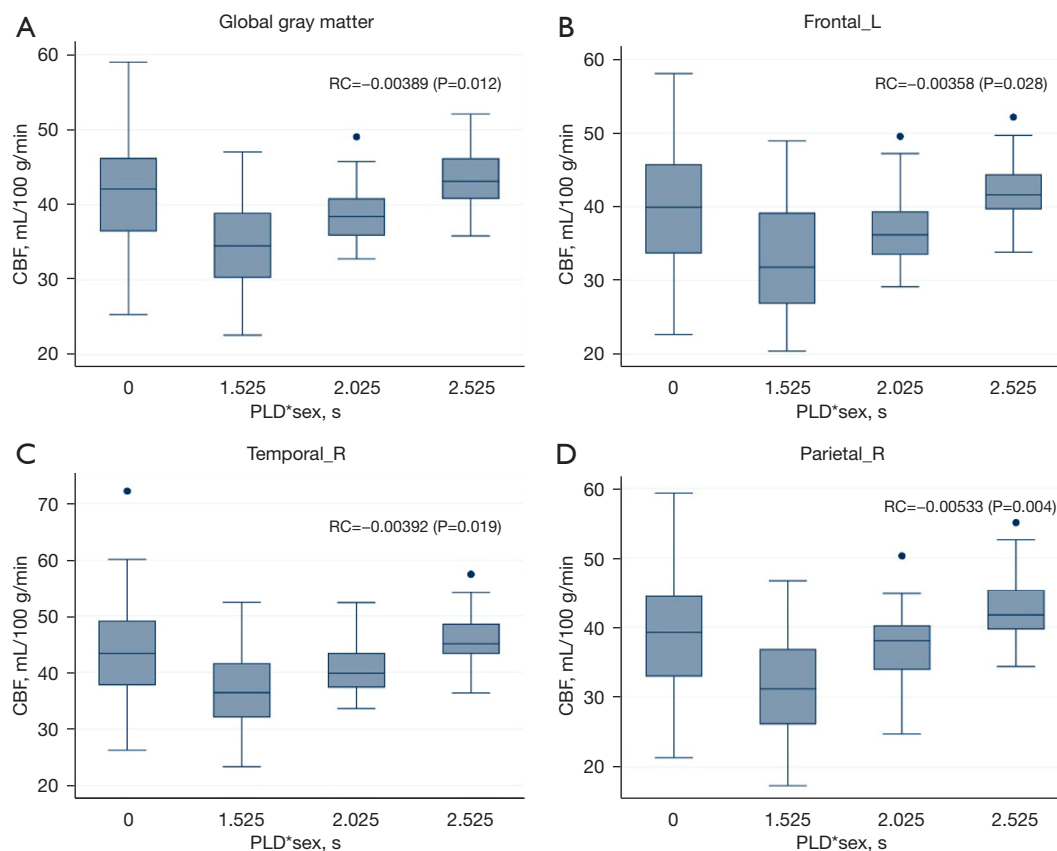
Figure 4 The boxplot of CBF values in some brain regions under different values of the interaction term (PLD*sex). In this study, the relationship between CBF and PLD can be expressed by the following equation: CBF = β_1PLD + β_2PLD*age + β_3PLD*sex. Females are assigned a value of 0 and males are assigned a value of 1. Therefore, for females, the relationship between CBF and PLD can be expressed as: CBF = β_1PLD + β_2PLD*age; for males, the relationship between CBF and PLD can be expressed as: CBF = β_1PLD + β_2PLD*age + β_3PLD. Thus, for the same age, the variation of CBF with PLD in female is determined by the regression coefficient β_1, and the variation of CBF with PLD in male is determined by the regression coefficient β_1 plus β_3. The figure shows that the regression coefficient β_1 in the global gray matter (A), left frontal lobe (B), right temporal lobe (C), right parietal lobe (D) were positive, and the regression coefficient β_3 were negative, so in these brain regions, the changes of CBF with PLD in females were greater than that of males. The black dots in this figure were discrete values. CBF, cerebral blood flow; PLD, post-labeling delay; RC, regression coefficient.

The effect of ATT on CBF

In this study, we found that CBF decreased with the increase of ATT in global gray matter (β=−208.635), all brain lobes (β ranged from −196.674 to −267.869) and the vascular territories of the anterior, middle, and posterior carotid artery (β ranged from −1.236 to −3.502). The interaction term (ATT*PLD) was positively significant in the above regions (β ranged from 0.000205 to 0.1135). Therefore, we may think that the effect of ATT on CBF was less influenced by PLD, because the regression coefficient of

the interaction term (ATT*PLD) was much smaller than the regression coefficient of ATT. The detailed regression coefficients are listed in Table S4.

The effect of ATT, PLD, age, and sex on spatial CoV

The spatial CoV in the global gray matter (β=11.614), bilateral frontal and temporal lobes (β ranged from 10.693 to 15.552), bilateral vascular territories of anterior carotid artery, and left vascular territory of middle carotid artery (β ranged from 0.089 to 0.136) were increased with the

increase of ATT. The spatial CoV in all brain lobes and the vascular territory of anterior, middle, and posterior carotid artery were decreased with the increase of PLD (β ranged from –0.02 to –0.00007). In addition, the spatial CoV in bilateral frontal, limbic lobes, left lateral occipital lobe, and left territory of posterior carotid artery were increased with age (β ranged from 0.051 to 0.091). The spatial CoV in bilateral temporal and right lateral occipital lobes were positively related to sex (β ranged from 1.445 to 2.354). The detailed regression coefficients are presented in Table S5.

Discussion

In this study, we conducted 3D pCASL imaging with 3 commonly used PLDs and performed multivariate regression analysis to investigate the potential influence of age and sex on the effect of PLD on CBF. Our findings demonstrated that among the ranges of PLDs we adopted, the CBF in the global gray matter, bilateral frontal, temporal lobes, and the vascular territories of bilateral anterior and middle carotid artery increased with PLD increasing, and younger individuals and females showed a more pronounced increase in CBF with PLD increasing. However, the CBF in the bilateral limbic lobes, insula, and deep gray matter decreased with PLD increasing, and older individuals and males exhibited a more pronounced decrease in CBF with PLD increasing.

Previous studies have also shown that the PLD affected CBF (42,43). However, the specific effect of PLD on CBF remains to be fully elucidated, as previous related studies are scarce and have often relied on the group comparisons (24,43). However, the interpretability of the results obtained from group comparisons was limited because this method does not control for variables such as age and sex. Therefore, in this study, we employed a combined regression analysis with ANOVA to investigate the effect of PLD on CBF. Previous studies have emphasized that the impact of PLD on CBF may be influenced by age and sex (33). However, there was scanty research analyzing how the effect of PLD on CBF was influenced by age and sex. The results of our study indicated that the increase of CBF with PLD was more pronounced in younger individuals and females in most brain regions, whereas the decrease of CBF with PLD was more pronounced in elderly individuals and males in few brain regions. Hence, optimizing the PLD for ASL may hold greater significance for young individuals and females.

In addition, the ANOVA showed that the among the 3 PLDs we used, most cortical brain regions showed the highest CBF value when the PLD was longest (2,525 ms), whereas the limbic lobes, insula, and deep gray matter showed the highest CBF value when the PLD was shortest (1,525 ms). This may be due to the ATT changes depending on the region of the brain. The ATT in most cortical regions is longer than the limbic lobe, insula, and deep gray matter (25,44). Hendrikse *et al.* also reported an increase in ATT in the cerebral border zone regions, extending from the frontal and occipital horns of the lateral ventricle to the frontal and parietooccipital cortices, relative to ATT in non-border zone regions (26).

Ideally, in ASL imaging, we want the PLD to match the ATT. If PLD < ATT, the labeled spins are still in the arteries and the images do not reflect tissue perfusion. If PLD > ATT, the labeling decay may result in lower signal-to-noise ratio. Therefore, when the PLD is shorter or longer than the ATT, the CBF may be underestimated (45,46); only when CBF initially increases and then decreases, with a turning point corresponding to the maximum CBF, can we accurately determine the optimal PLD. However, in our research, only the CBF gradually increased as the PLD increased, or the CBF gradually decreased as the PLD increased, or CBF showed the trend of lowering first and then increasing. Therefore, we could only speculate that 2,525 ms may be the best PLD for the ASL imaging in most cortical brain regions, especially among the middle-aged and elderly people. In addition, we speculated that 1,525 ms may be the best PLD for the ASL imaging in limbic lobe, insula, and subcortical brain regions, especially among the young people. More longer and shorter PLDs need to be included to verify the optimal PLD which we speculated in our study.

Our study demonstrated that the CBF in all brain regions decreased with aging and the CBF was higher for females compared to males. These findings are consistent with previous research (47-53). In previous research (54), we found that CBF in the global gray matter and most brain regions exhibited a non-linear decrease with age, and the rate of CBF reduction decreased with aging. Since this study primarily focused on whether age affects the impact of PLD on CBF, age was included as a control variable and as one of the interaction terms. Therefore, the study did not specifically investigate the nonlinear relationship between age and CBF. Previous studies have indicated that an age-related CBF decrease is mainly or exclusively a consequence

of reduced metabolic needs (55-57). The reasons for sex differences in CBF were not fully understood, yet several possible explanations have been proposed. A possible explanation was the variation in hematocrit levels between sex (47,58,59). Another explanation is related to differences in metabolic rate and brain size. It has been suggested that females have higher metabolic rates and relatively smaller brain sizes compared to males, which may result in higher CBF per 100 g of brain tissue in females (60,61). In addition, the effects of age and sex on CBF may attribute to the effects of age and sex on ATT. We found that the ATT of all brain regions increased with aging, and the ATT of most brain regions was higher in males. Also, our study showed that the CBF decreased with the increase of ATT in all brain regions. This may be due to the fact that the longer the ATT, the less labeling blood flow arriving to the imaging level under the same PLD, thus resulting in a lower CBF (45,46).

In our study, the spatial CoV increased with the increase of ATT, decreased with the increase of PLD, increased with aging, and was greater in males. Many studies show ASL image heterogeneity between participants that is attributed to ATT artifacts that usually appeared due to the mismatch of ATT and PLD (32). Therefore, our results may indicate that more serious ATT artifacts may occur with the increase of ATT, age, the decrease of PDL, and for males.

This study has some limitations. First, this study only included adults; the conclusions of this study may not be applicable to children. Second, we included only healthy volunteers; patients such as those with impaired blood flow were not included. Third, we only performed 3 PLDs because our total acquisition time was nearly half an hour which was the longest imaging time many volunteers could accept. Based on our preliminary experiments, it was observed that most volunteers were able to maintain a stationary position for up to 30 minutes. However, it is important to note that the 3 PLDs used in this study are commonly employed in current research. Nevertheless, to further validate the results of this study, it would be beneficial to include additional PLDs. Another limitation is that MRI scanning was performed on only 1 machine in our study. Due to the impact of multi-vendor variations, the reproducibility of our findings on other vendors needs to be further studied. Finally, although we did our best to collect a relatively large sample of normal adults, the sample size of each subgroup was relatively small after these participants were divided into young, middle-aged, and elderly groups.

Conclusions

When using ASL imaging, the obtained CBF is affected by the PLD. Furthermore, the impact of PLD on CBF is influenced by age and sex, with younger individuals and females showing a greater effect of PLD on CBF in most brain regions. Therefore, young individuals and females are more sensitive to changes in PLD when measuring CBF using ASL.

Acknowledgments

Footnote

References

1. Biagi L, Abbruzzese A, Bianchi MC, Alsop DC, Del

4400

Hu et al. Age and sex influence the effect of PLD on CBF

Guerra A, Tosetti M. Age dependence of cerebral perfusion assessed by magnetic resonance continuous arterial spin labeling. J Magn Reson Imaging 2007;25:696-702.

2. Wang H, Chai C, Wu G, Li J, Zhao C, Fu D, Zhang S, Wang H, Wang B, Zhu J, Shen W, Xia S. Cerebral blood flow regulates iron overload in the cerebral nuclei of hemodialysis patients with anemia. J Cereb Blood Flow Metab 2023;43:749-62.

3. van Dinther M, Hooghiemstra AM, Bron EE, Versteeg A, Leeuwis AE, Kalay T, Moonen JE, Kuipers S, Backes WH, Jansen JFA, van Osch MJP, Biessels GJ, Staals J, van Oostenbrugge RJ; . Lower cerebral blood flow predicts cognitive decline in patients with vascular cognitive impairment. Alzheimers Dement 2024;20:136-44.

4. Mitchell RHB, Grigorian A, Robertson A, Toma S, Luciw NJ, Karthikeyan S, Mutsaerts HJMM, Fiksenbaum L, Metcalfe AWS, MacIntosh BJ, Goldstein BI. Sex differences in cerebral blood flow among adolescents with bipolar disorder. Bipolar Disord 2024;26:33-43.

5. Percie du Sert O, Unrau J, Gauthier CJ, Chakravarty M, Malla A, Lepage M, Raucher-Chéné D. Cerebral blood flow in schizophrenia: A systematic review and meta-analysis of MRI-based studies. Prog Neuropsychopharmacol Biol Psychiatry 2023;121:110669.

6. Huang D, Guo Y, Guan X, Pan L, Zhu Z, Chen Z, Dijkhuizen RM, Duering M, Yu F, Boltze J, Li P. Recent advances in arterial spin labeling perfusion MRI in patients with vascular cognitive impairment. J Cereb Blood Flow Metab 2023;43:173-84.

7. van der Thiel M, Rodriguez C, Giannakopoulos P, Burke MX, Lebel RM, Gninenko N, Van De Ville D, Haller S. Brain Perfusion Measurements Using Multidelay Arterial Spin-Labeling Are Systematically Biased by the Number of Delays. AJNR Am J Neuroradiol 2018;39:1432-8.

8. van Grinsven EE, Guichelaar J, Philippens ME, Siero JC, Bhogal AA. Hemodynamic imaging parameters in brain metastases patients - Agreement between multi-delay ASL and hypercapnic BOLD. J Cereb Blood Flow Metab 2023;43:2072-84.

9. Alsop DC, Detre JA, Golay X, Günther M, Hendrikse J, Hernandez-Garcia L, Lu H, MacIntosh BJ, Parkes LM, Smits M, van Osch MJ, Wang DJ, Wong EC, Zaharchuk G. Recommended implementation of arterial spin-labeled perfusion MRI for clinical applications: A consensus of the ISMRM perfusion study group and the European consortium for ASL in dementia. Magn Reson Med 2015;73:102-16.

10. Lindner T, Bolar DS, Achten E, Barkhof F, Bastos-Leite AJ, Detre JA, et al. Current state and guidance on arterial spin labeling perfusion MRI in clinical neuroimaging. Magn Reson Med 2023;89:2024-47.

11. Wang H, Han X, Li M, Yang ZH, Liu WH, Wang ZC. Long-term hemodialysis may affect enlarged perivascular spaces in maintenance hemodialysis patients: evidence from a pilot MRI study. Quant Imaging Med Surg 2022;12:341-53.

12. Luo J, Feng Y, Lu X, Fang S, Zheng S, Zeng G, Yan L, Yang B, Wang T, Jiao L, Luo Y, Han Z, Ma Y. Potential of unilateral combined bypass surgery to accelerate contralateral radiological progression in pediatric moyamoya disease. Quant Imaging Med Surg 2023;13:6615-26.

13. Gai ND, Butman JA. Determining the optimal postlabeling delay for arterial spin labeling using subject-specific estimates of blood velocity in the carotid artery. J Magn Reson Imaging 2019;50:951-60.

14. Petersen ET, Lim T, Golay X. Model-free arterial spin labeling quantification approach for perfusion MRI. Magn Reson Med 2006;55:219-32.

15. Wong EC, Buxton RB, Frank LR. Implementation of quantitative perfusion imaging techniques for functional brain mapping using pulsed arterial spin labeling. NMR Biomed 1997;10:237-49.

16. Fujiwara Y, Matsuda T, Kanamoto M, Tsuchida T, Tsuji K, Kosaka N, Adachi T, Kimura H. Comparison of long-labeled pseudo-continuous arterial spin labeling (ASL) features between young and elderly adults: special reference to parameter selection. Acta Radiol 2017;58:84-90.

17. Kindler J, Schultze-Lutter F, Hauf M, Dierks T, Federspiel A, Walther S, Schimmelmann BG, Hubl D. Increased Striatal and Reduced Prefrontal Cerebral Blood Flow in Clinical High Risk for Psychosis. Schizophr Bull 2018;44:182-92.

18. Barzgari A, Sojkova J, Maritza Dowling N, Pozorski V, Okonkwo OC, Starks EJ, Oh J, Thiesen F, Wey A, Nicholas CR, Johnson S, Gallagher CL. Arterial spin labeling reveals relationships between resting cerebral perfusion and motor learning in Parkinson's disease. Brain Imaging Behav 2019;13:577-87.

19. Madhyastha TM, Askren MK, Boord P, Zhang J, Leverenz JB, Grabowski TJ. Cerebral perfusion and cortical thickness indicate cortical involvement in mild Parkinson's disease. Mov Disord 2015;30:1893-900.

20. Zhu J, Zhuo C, Xu L, Liu F, Qin W, Yu C. Altered Coupling Between Resting-State Cerebral Blood Flow and Functional Connectivity in Schizophrenia. Schizophr Bull

2017;43:1363-74.

21. Huang J, Hao P, Chen Z, Deng K, Liu B, Xu Y. Quantitative assessment of hyperperfusion using arterial spin labeling to predict hemorrhagic transformation in acute ischemic stroke patients with mechanical endovascular therapy. Eur Radiol 2024;34:579-87.

22. Meng M, Liu F, Ma Y, Qin W, Guo L, Peng S, Gordon ML, Wang Y, Zhang N. The identification and cognitive correlation of perfusion patterns measured with arterial spin labeling MRI in Alzheimer's disease. Alzheimers Res Ther 2023;15:75.

23. Zakharova NE, Batalov AI, Pogosbekian EL, Chekhonin IV, Goryaynov SA, Bykanov AE, Tyurina AN, Galstyan SA, Nikitin PV, Fadeeva LM, Usachev DY, Pronin IN. Perifocal Zone of Brain Gliomas: Application of Diffusion Kurtosis and Perfusion MRI Values for Tumor Invasion Border Determination. Cancers (Basel) 2023;15:2760.

24. Hu Y, Li Q, Chen L, Lv F. Multidelay arterial spin-labeled perfusion magnetic resonance imaging in healthy individuals: A single-center experience. Neurol India 2019;67:829-33.

25. Sanvito F, Palesi F, Rognone E, Barzaghi L, Pasca L, Germani G, De Giorgis V, Borgatti R, Gandini Wheeler-Kingshott CAM, Pichiecchio A. Impact of the inversion time on regional brain perfusion estimation with clinical arterial spin labeling protocols. MAGMA 2022;35:349-63.

26. Hendrikse J, Petersen ET, van Laar PJ, Golay X. Cerebral border zones between distal end branches of intracranial arteries: MR imaging. Radiology 2008;246:572-80.

27. Dai W, Robson PM, Shankaranarayanan A, Alsop DC. Reduced resolution transit delay prescan for quantitative continuous arterial spin labeling perfusion imaging. Magn Reson Med 2012;67:1252-65.

28. Mildner T, Müller K, Hetzer S, Trampel R, Driesel W, Möller HE. Mapping of arterial transit time by intravascular signal selection. NMR Biomed 2014;27:594-609.

29. Li Y, Wang Z. Deeply Accelerated Arterial Spin Labeling Perfusion MRI for Measuring Cerebral Blood Flow and Arterial Transit Time. IEEE J Biomed Health Inform 2023;27:5937-45.

30. Zhao MY, Armindo RD, Gauden AJ, Yim B, Tong E, Moseley M, Steinberg GK, Zaharchuk G. Revascularization improves vascular hemodynamics - a study assessing cerebrovascular reserve and transit time in Moyamoya patients using MRI. J Cereb Blood Flow Metab 2023;43:138-51.

31. Yu H, Ouyang Y, Feng Y, Sun S, Zhang L, Liu Z, Tian H, Xie S. Comparison of single-postlabeling delay and seven-

delay three-dimensional pseudo-continuous arterial spin labeling in the assessment of intracranial atherosclerotic disease. Quant Imaging Med Surg 2023;13:2514-25.

32. Mutsaerts HJ, Petr J, Václavů L, van Dalen JW, Robertson AD, Caan MW, Masellis M, Nederveen AJ, Richard E, MacIntosh BJ. The spatial coefficient of variation in arterial spin labeling cerebral blood flow images. J Cereb Blood Flow Metab 2017;37:3184-92.

33. Wang Z, Aguirre GK, Rao H, Wang J, Fernández-Seara MA, Childress AR, Detre JA. Empirical optimization of ASL data analysis using an ASL data processing toolbox: ASLtbx. Magn Reson Imaging 2008;26:261-9.

34. Ashburner J, Friston KJ. Unified segmentation. Neuroimage 2005;26:839-51.

35. Wang R, Yu S, Alger JR, Zuo Z, Chen J, Wang R, An J, Wang B, Zhao J, Xue R, Wang DJ. Multi-delay arterial spin labeling perfusion MRI in moyamoya disease--comparison with CT perfusion imaging. Eur Radiol 2014;24:1135-44.

36. Zaharchuk G, Straka M, Marks MP, Albers GW, Moseley ME, Bammer R. Combined arterial spin label and dynamic susceptibility contrast measurement of cerebral blood flow. Magn Reson Med 2010;63:1548-56.

37. Qiu D, Straka M, Zun Z, Bammer R, Moseley ME, Zaharchuk G. CBF measurements using multidelay pseudocontinuous and velocity-selective arterial spin labeling in patients with long arterial transit delays: comparison with xenon CT CBF. J Magn Reson Imaging 2012;36:110-9.

38. Tatu L, Moulin T, Bogousslavsky J, Duvernoy H. Arterial territories of the human brain: cerebral hemispheres. Neurology 1998;50:1699-708.

39. Berman SA, Hayman LA, Hinck VC. Correlation of CT cerebral vascular territories with function: I. Anterior cerebral artery. AJR Am J Roentgenol 1980;135:253-7.

40. Hayman LA, Berman SA, Hinck VC. Correlation of CT cerebral vascular territories with function: II. Posterior cerebral artery. AJR Am J Roentgenol 1981;137:13-9.

41. Berman SA, Hayman LA, Hinck VC. Correlation of CT cerebral vascular territories with function: 3. Middle cerebral artery. AJR Am J Roentgenol 1984;142:1035-40.

42. Bland JM, Altman DG. Multiple significance tests: the Bonferroni method. BMJ 1995;310:170.

43. Staffa SJ, Zurakowski D. Strategies in adjusting for multiple comparisons: A primer for pediatric surgeons. J Pediatr Surg 2020;55:1699-705.

44. Pinto J, Chappell MA, Okell TW, Mezue M, Segerdahl AR, Tracey I, Vilela P, Figueiredo P. Calibration of arterial

Quant Imaging Med Surg 2024;14(7):4388-4402 | https://dx.doi.org/10.21037/qims-23-1622

spin labeling data-potential pitfalls in post-processing. Magn Reson Med 2020;83:1222-34.

45. Buxton RB, Frank LR, Wong EC, Siewert B, Warach S, Edelman RR. A general kinetic model for quantitative perfusion imaging with arterial spin labeling. Magn Reson Med 1998;40:383-96.

46. Alsop DC, Detre JA. Reduced transit-time sensitivity in noninvasive magnetic resonance imaging of human cerebral blood flow. J Cereb Blood Flow Metab 1996;16:1236-49.

47. Woods JG, Chappell MA, Okell TW. A general framework for optimizing arterial spin labeling MRI experiments. Magn Reson Med 2019;81:2474-88.

48. MacIntosh BJ, Filippini N, Chappell MA, Woolrich MW, Mackay CE, Jezzard P. Assessment of arterial arrival times derived from multiple inversion time pulsed arterial spin labeling MRI. Magn Reson Med 2010;63:641-7.

49. Wu WC, Fernández-Seara M, Detre JA, Wehrli FW, Wang J. A theoretical and experimental investigation of the tagging efficiency of pseudocontinuous arterial spin labeling. Magn Reson Med 2007;58:1020-7.

50. Fahlström M, Lewén A, Enblad P, Larsson EM, Wikström J. High Intravascular Signal Arterial Transit Time Artifacts Have Negligible Effects on Cerebral Blood Flow and Cerebrovascular Reserve Capacity Measurement Using Single Postlabel Delay Arterial Spin-Labeling in Patients with Moyamoya Disease. AJNR Am J Neuroradiol 2020;41:430-6.

51. Liu Y, Zhu X, Feinberg D, Guenther M, Gregori J, Weiner MW, Schuff N. Arterial spin labeling MRI study of age and gender effects on brain perfusion hemodynamics. Magn Reson Med 2012;68:912-22.

52. Chen JJ, Rosas HD, Salat DH. Age-associated reductions in cerebral blood flow are independent from regional atrophy. Neuroimage 2011;55:468-78.

53. Galiano A, Mengual E, García de Eulate R, Galdeano I, Vidorreta M, Recio M, Riverol M, Zubieta JL, Fernández-Seara MA. Coupling of cerebral blood flow and functional connectivity is decreased in healthy aging. Brain Imaging Behav 2020;14:436-50.

54. Soni N, Jain A, Kumar S, Pandey CM, Awasthi A. Arterial spin labeling magnetic resonance perfusion study to evaluate the effects of age and gender on normal cerebral blood flow. Neurol India 2016;64 Suppl:S32-8.

55. Daniel DG, Mathew RJ, Wilson WH. Sex roles and regional cerebral blood flow. Psychiatry Res 1989;27:55-64.

56. Hales PW, Kawadler JM, Aylett SE, Kirkham FJ, Clark CA. Arterial spin labeling characterization of cerebral perfusion during normal maturation from late childhood into adulthood: normal 'reference range' values and their use in clinical studies. J Cereb Blood Flow Metab 2014;34:776-84.

57. Gur RE, Gur RC. Gender differences in regional cerebral blood flow. Schizophr Bull 1990;16:247-54.

58. Hu Y, Liu R, Gao F. Arterial Spin Labeling Magnetic Resonance Imaging in Healthy Adults: Mathematical Model Fitting to Assess Age-Related Perfusion Pattern. Korean J Radiol 2021;22:1194-202.

59. Shefer VF. Absolute number of neurons and thickness of the cerebral cortex during aging, senile and vascular dementia, and Pick's and Alzheimer's diseases. Neurosci Behav Physiol 1973;6:319-24.

60. Henderson G, Tomlinson BE, Gibson PH. Cell counts in human cerebral cortex in normal adults throughout life using an image analysing computer. J Neurol Sci 1980;46:113-36.

61. BRODY H. Organization of the cerebral cortex. III. A study of aging in the human cerebral cortex. J Comp Neurol 1955;102:511-6.